Talanta 239 (2022) 123092

Contents lists available at ScienceDirect

Talanta

journal homepage: www.elsevier.com/locate/talanta

Protein biosensor based on Schottky barrier nanowire field effect transistor

Tatyana E. Smolyarova [a,b,d,*], Lev V. Shanidze [a,b], Anna V. Lukyanenko [a,d], Filipp A. Baron [a], Vasilisa V. Krasitskaya [c], Anna S. Kichkailo [b,e], Anton S. Tarasov [a,d], Nikita Volkov [a]

[a] Kirensky Institute of Physics, Federal Research Center KSC SB RAS, Krasnoyarsk, 660036, Russia
[b] Federal Research Center KSC SB RAS, Krasnoyarsk, 660036, Russia
[c] Institute of Biophysics, Federal Research Center KSC SB RAS, Krasnoyarsk, 660036, Russia
[d] Siberian Federal University, Krasnoyarsk, 660041, Russia
[e] Krasnoyarsk State Medical University, Krasnoyarsk, 660022, Russia

ARTICLE INFO

Keywords:
Silicon-on-insulator
Schottky contacts FET
Si nanowire biosensor
Back gate nanowire FET

ABSTRACT

A top-down nanofabrication approach involving molecular beam epitaxy and electron beam lithography was used to obtain silicon nanowire-based back gate field-effect transistors with Schottky contacts on silicon-on-insulator (SOI) wafers. The resulting device is applied in biomolecular detection based on the changes in the drain-source current (I_{DS}). In this context, we have explained the physical mechanisms of charge carrier transport in the nanowire using energy band diagrams and numerical 2D simulations in TCAD. The results of the experiment and numerical modeling matched well and may be used to develop novel types of nanowire-based biosensors.

1. Introduction

Nanometer-scale structures, in particular silicon nanowires (SiNWs), attract considerable attention for sensors applications. Many research groups have demonstrated the exciting potential of silicon nanowires for use as novel biosensors [1,2]. Specifically, silicon nanowires are widely used in integrated nanoscale electronics, such as complementary oxide-metal semiconductors (CMOS) [3–5], also in lab-on-chip devices [6–8] for label-free [9,10] and high sensitivity detection [11,12]. Furthermore, biosensors based on nanowire field-effect transistors (FETs) with Schottky contacts are under intensive investigations as an alternative to traditional doped source and drain device structures [13–15]. In addition, Schottky barrier FETs have many advantages, including a straightforward low temperature processing, good suppression of short channel effects, and the elimination of doping and subsequent activation steps [16]. These features are particularly desirable for SiNW devices because they can circumvent complex fabrication issues such as accurate control of the doping type/level and the formation of reliable Ohmic contacts.

Although there are many of available works about biosensors based on silicon nanowire field-effect transistors with Schottky contacts, physical mechanisms of charge carrier transport in a nanowire have not been explained in detail. Usually, the experimental investigations of SiNW biosensors based on the back gate field-effect transistors with Schottky contacts are focused on the study of the sensitivity of a fabricated device [17,18] or surface modifications and molecular targets [19,20]. Existing theoretical investigations related to silicon nanowire-based field-effect transistors partially explain physical principles of charge carrier transport occurring at the moment of a molecule detection in the gate all around Silicon NWFET [21,22], nanowire ISFET [23–25], and MOSFET [26] based biosensors. At the same time, detailed reports on the theoretical and experimental study of carrier transport in silicon nanowire-based back gate field-effect transistors with Schottky contacts on SOI wafers depending on the charge of the attached targets are missing. However, particular insight into the physical mechanisms acting when a silicon nanowire is used as a sensor element may lead to the fabrication of outstanding highly sensitive nanowire-based biosensors. The most popular way for implementing such devices in nanoscale is the "top-down" synthesis approach [27–29], which allows the definition of device geometry and electrical characteristics due to precise control of lateral sizes of a nanowire. It enables direct contact with other structures on a device, compared with the "bottom-up" approach, which usually uses chemical methods to obtain nanostructures [30–32] that are incapable of controlling geometrical characteristics. This paper focuses on studying of the experimental and numerically simulated performance of the protein biosensor-based

* Corresponding author. Kirensky Institute of Physics, Federal Research Center KSC SB RAS, Krasnoyarsk, 660036, Russia.
E-mail address: smol.nano@yandex.ru (T.E. Smolyarova).

https://doi.org/10.1016/j.talanta.2021.123092
Received 22 August 2021; Received in revised form 18 November 2021; Accepted 22 November 2021
Available online 24 November 2021

silicon nanowire back gate field-effect transistor with Schottky contacts fabricated by technology involving electron-beam lithography process combined with reactive ion and wet chemical etching.

2. Materials and methods

Silicon-on-Insulator (SOI) (100) wafers with 200 nm thick buried oxide (BOX) and 100-nm monocrystalline top boron-doped silicon device layer (with resistivity of 18 Ω cm), AZ 2035 nLof resist were used for SiNW FET fabrication. 3-Aminopropyltriethoxysilane (APTES), N,N-Bis (2-hydroxyethyl)glycine (BICINE), dimethyl suberimidate dihydrochloride (DMS), bovine serum albumin (BSA) were from Sigma. The recombinant streptavidin used for SiNW surface modification was produced as described in Ref. [33]. Biotin-labeled bovine serum albumin (Biotin-BSA) was obtained by reaction with 20-M excess of succinimide derivative of biotin (Pierce, USA), followed by removal of the excess reagent by gel filtration. Lithographical steps were performed using the Raith Voyager e-beam writer and NORDSON MARCH RIE-1701 anisotropic reactive ion etch plasma system. Iron polycrystalline metal contact pads (14 nm) were grown at 400 K by thermal evaporation from Knudsen cells under ultra-high vacuum conditions (10^{-8} Pa) (UHV). The surface morphology of the fabricated SiNWs and the quality of produced iron film were characterized using NanoInk DPN 5000 atomic-force microscope, Hitachi S-5500 and Hitachi TM-3000 scanning electron microscopes. Transfer characteristics of prepared devices were measured using Keithley 2634b SourceMeter. Investigations of DC charge carrier transport were carried out at probe station Lakeshore EMPX-HF 2.

2.1. Biosensor fabrication

The nanofabrication process of Schottky barrier SiNW FET using the "top-down" approach represents a multistep process, which was fully described in Refs. [34,35] (Fig. 1(a)). Firstly, the SOI wafer was cleaned to remove contaminants and native oxide. After the cleaning procedure, metal contact pads for carrying out the investigations of electric properties were obtained using thermal evaporation under UHV and Electron Beam Lithography (EBL) exposure process combined with wet chemical etching and reactive ion etching (RIE) was used to obtain a nanowire from the SOI device layer. The result of described technological process is an array of silicon nanowire structures on a dielectric layer with metal pads of the source (S) and drain (D) connected to the ends of fabricated nanowires for subsequent electrical properties measurements. In addition, besides the metal pads (S and D) for the measurement of electrical properties of the fabricated structure a back gate was made on the backside of the SOI substrate using doping with indium (In). The thin silicon device layer represents the transistor body, and the buried oxide serves as the gate insulator. The thick SiO_2 layer plays the role of the gate and can be biased by In-doped back contact to induce a conducting channel at the interface between the Si device layer and the buried oxide. Depending on the positive or negative "back-gate" bias, an inversion or accumulation channel can be activated in the transistor body.

2.2. SiNW surface functionalization

Functionalization of the SiNW surface is a necessary step to evaluate the performance of manufactured devices. Fig. 1 (b) represents the schematic diagram of the SiNW surface functionalization process. First, we applied the silanization reaction by APTES (50% aqueous solution),

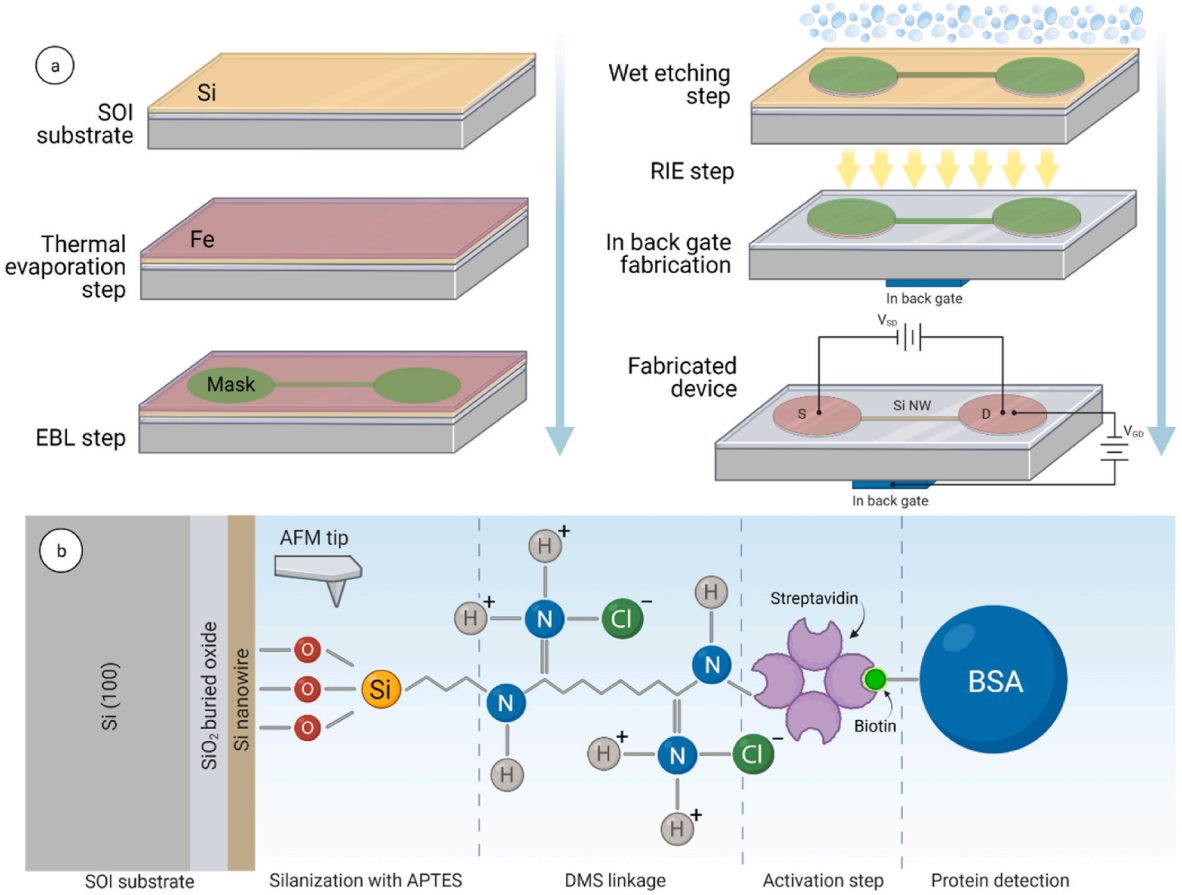

Fig. 1. (a) Multistep process of SiNW FET nanowire fabrication; (b) Biotin-BSA immobilization to SiNW surface.

which is covalently bound to the SiNW surface through the siloxane bonds (Si–O–Si) formation resulting in activation of SiNWs surface by amino groups for further covalent immobilization of recognition biomolecules. Amino groups were introduced on the SiNW surface by silanization reaction with APTES, 98%. To ensure accurate/precise coverage of SiNW surface APTES molecules were deposited onto a SiNW surface using the probe of an atomic-force microscope under the following conditions T = 24.2 °C, PH = 52.1%. As a recognition molecule in our model experiment streptavidin was used. After washing the surface with (0.1 M Bicine pH 8.5) 2 μl of streptavidin (1 mg/ml) and 0.5 μl of homobifunctional crosslinker DMS (50 mg/ml) in 0.1 M Bicine pH 8.5 were dropped on the SiNW surface and incubated in a humid environment for 20 min. This way streptavidin was covalently attached to NH_2-activated SiNW surface using an excess of homobifunctional crosslinker DMS reactive toward amino groups (Fig. 1 (b)).

Then the SiNW surface was washed by Twin buffer, containing PBS and 0.1% Tween20. Streptavidin is a homotetrameric protein produced by *Streptomyces avidinii*, each subunit of which binds biotin (vitamin H), forming one of the most stable noncovalent complexes known in nature (Kd = 10^{-15} M). Due to that streptavidin-biotin interaction is extensively used in molecular biology and bionanotechnology [36]. As a target molecule we applied biotinylated bovine serum albumin. For this purpose, 2 μl of Biotin-BSA (0.1 M Bicine pH 8.5 buffer) were dropped on the SiNW surface, incubated for 20 min and then the sample surface was washed with Twin buffer (Fig. 1 (b)). After each stage of SiNW surface functionalization the current-voltage (I–V) characteristic between the source (S) and drain (D) contact pads were measured.

3. Results and discussion

The grown iron polycrystalline film was analyzed using transmission electron microscopy (TEM) to confirm the morphological homogeneity ensure the metal contact pads conductivity (Fig. 2(b)). Firstly, there is no oxide or other interlayer between Fe film and silicon device layer. Secondly, the iron film is entirely homogeneous, has a thickness of 14 nm, and has no defects to influence the transfer characteristics of fabricated FET's. Scanning electron microscopy (SEM) analyses were performed to examine the chemical etching step quality, the contact of metal pads with SiNW and surface morphology of fabricated SiNWs (Fig. 2(c)). The thickness and surface morphology of fabricated SiNWs were examined by atomic-force microscopy (AFM) (Fig. 2(d)). The results confirm the quality of the etching process performed after the iron film growth when the sample with AZ 2035 nLof resist protected mask was slightly overexposed in wet reactant to dissolve iron under a protective mask for only 1 μm from the edges of the resist. This way, the second lithography step for the *Si*-nanowire definition was not needed. Indeed, the exposed photoresist mask remained on top of the active device (nanowire) areas, which was enough to proceed with the anisotropic dry etching step and remove the top silicon layer from open areas using CF_4 reactive plasma followed by the remaining resist dissolution in acetone. As a result, we see bare silicon nanowires with iron contact pads on S/D-contacts areas only.

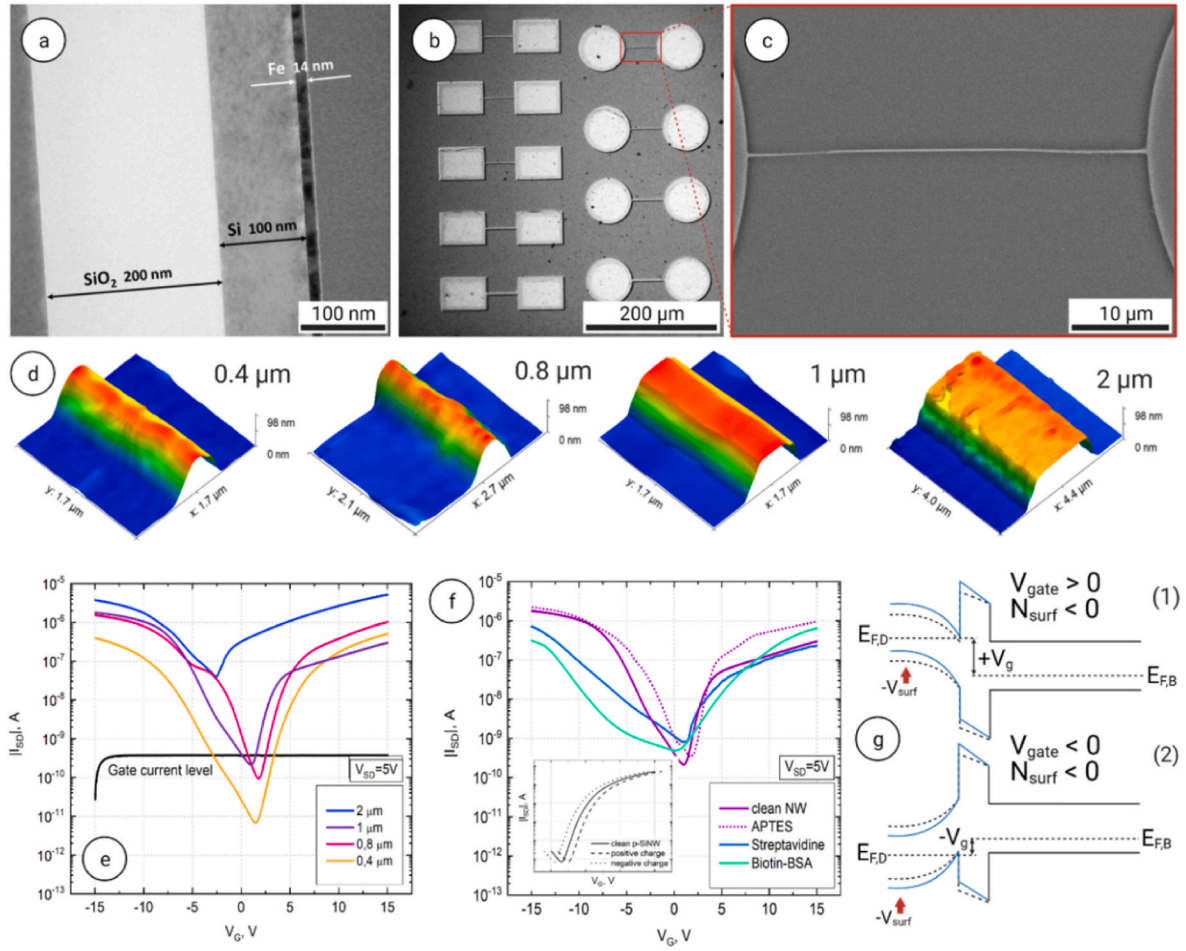

Fig. 2. (a) TEM image of SOI substrate with grown iron polycrystalline film; (b) optical image of fabricated SiNW FETs and (c) SEM image of fabricated 0,4 μm SiNW; (d) AFM scans of 0.4 μm, 0.8 μm, 1 μm, 2 μm SiNWs; (e) transfer characteristics of fabricated devices at the source bias V_{SD} = 5 V ($I_G(V_G)$ gate current level presented as a black curve); (f) comparison of transfer characteristics of fabricated biosensors for different steps of nanowire surface modification; (g) band diagrams of (1) inversion and (2) accumulation modes of fabricated device.

3.1. Electrical performance of fabricated SiNW FET

The current-voltage (I–V) characteristic between the source (S) and drain (D) contact pads were measured before surface functionalization of silicon nanowires with APTES molecules. The I_{SD}-V_{GD} characteristics for nanowires with 0.4, 0.8, 1 and 2 μm widths are presented in Fig. 2 (e). These characteristics show that the behavior of the fabricated device is analogous to an enhancement mode device transistor [37]. The current appears because of the accumulation of the holes, as majority carriers, in the p-doped SiNW on the Si/SiO_2 interface when the channel is formed. In this matter, SiNW FET normally is closed, since the silicon layer is lightly doped (of the order of 10^{15} cm^{-3}), a very high resistance at zero gate voltage occurs. Moreover, as the source and drain are made as Schottky contacts, the resistance of the transistor in a current mode is additionally increased in this device. These characteristics confirm the high quality of the top-down nanofabrication process for the production of silicon nanowires with great potential for further development.

3.2. Detection of Biotin-BSA by SiNW FET

When a detectable molecule is deposited on the surface of a nanowire, it acts as a floating charged gate. Biotin-BSA deposition leads to a shift of the gate voltage characteristic towards the negative bias, while the overall behavior remains the same (Fig. 2 (f)). That means that the main physical mechanisms of charge carrier transport in the nanowire remain the same as for a pure device. However, the negative surface charge density causes the shift of the transfer characteristics towards negative bias on the silicon nanowire, as it was demonstrated for n-doped SiNWs in Ref. [38]. In the case of a p-doped SiNW the transfer characteristics shift to the opposite direction (right or left), depending on the charge of the detected molecule, as shown schematically in the insert in Fig. 2 (f). Indeed, streptavidin and Biotin-BSA are molecules with a negative charge [39], acting as a floating upper gate. According to the net charge of the protein in a solution with a pH above the isoelectric point is negative and BSA isoelectric point is 5.85, the net charge of the protein in the used solution with pH = 8.5 is negative. Upon the functionalization of the SiNW surface with neutral APTES molecules, a coordinate covalent bond appears. Therefore, a positive surface charge density appears on the surface of the silicon nanowire. In addition, when the Biotin-BSA is detected, there is a sharp decrease in the drain-source current: 2 orders of magnitude at −7 V at the gate in comparison with clean nanowire and 1 order of magnitude at the gate in comparison with streptavidin activated nanowire surface at negative biases, which can be used to implement a sensor (Fig. 2 (f)).

By the reason that the nanowire surface acquires a negative charge due to the protein attachment, the energy band bending is modulated by this extra charge, shifting the bands slightly upward. This up-shift translates into the current decrease in the inversion mode of the transistor as the conduction band edge at the Si/SiO_2 interface moves further up from the Fermi-level and the 2D electron gas concentration decreases (Figs. 2 (g-1)). Alternatively, the hole current increases in the accumulation mode since the valence band edge at the Si/SiO_2 interface moves deeper under the holes Fermi-level resulting in the 2D hole gas concentration increase (Fig. 2 (g-2)). Thus, the combined effect of the above two mechanisms is an effective positive shift of transistor IV-curve and associated device threshold voltage.

3.3. 2D simulation

For the quantitative analysis of the device performance depending on the sensor surface charge concentration, we carried out numerical 2D simulations of the back-gate SOI FET using TCAD. A self-consistent numerical solution of the voltage-defined boundary value problem for the Poisson, current continuity, and drift-diffusion partial differential equations system in quasi-stationary approximation have been implemented using Bank-Rose non-linear solver [40] with Scharfetter-Gummel discretization [41]. The carriers' concentration was determined using Boltzmann statistics and Caughey-Thomas high-field saturation model for the doping-dependent mobility. Electron and hole tunneling rates through the source/drain (S/D) contacts Schottky barriers were calculated using a non-local tunneling model [42,43]. To account for the effect of the native oxide layer on the tunneling rates in our simulations we included a 0.5 nm SiO_2 interlayer between the Si device layer and S/D metal contacts. Band-to-band tunneling current was taken into account using the Hurkx model [44]. Tunneling through the Schottky and SiO_2 interlayer barriers at S/D-contacts resulted in small and non-uniform currents and, thus, loosely defined boundary value problem for the electrostatic potential of the Si-device layer, which considerably impeded convergence and forced us to use a very fine mesh of the high-field current injection areas near the edges of the S/D tunneling junctions. Avalanche currents have been omitted for their detrimental effect on the convergence (Fig. 3 (a)).

Attachment of detectable molecules on the functionalized device surface was taken into account by considering an effective surface charge variation at the silicon-air interface affecting the FET threshold and on-current. Fig. 3 (a) shows the simulation results of the FET transfer characteristics drain current (I_D) versus gate voltage (V_{GS}) for different device surface charge concentrations. These IV-curves qualitatively match experimental data but require more profound insight into the nature of discrepancies observed. Therefore, we explored some basic parameters affecting their shape.

As the device is routinely exposed to different solutions, it may get contaminated with copper or other metallic deep-level impurities that create the recombination centers in the device layer. Shown in Fig. 3 (b, c) are the transfer IV-curves of the nanowire FET simulated for different carriers' lifetime within the framework of the Shockley-Reed-Hall recombination mechanism for two different bias values of the source terminal. These data show that the recombination lifetime variation can significantly modify the shape of the device characteristic at negative gate bias but has a negligible effect at positive V_{GS}.

Since the IV-curves shape modification was sensitive to the source bias voltage, we also explored the effect of the V_{SD} voltage with the other parameters kept fixed (Fig. 3 (d)). The data reveals non-monotonous behavior at negative gate voltages. At first, the drain current decreases reaching values in the 10s of fA range, but then it bounces back as we increase the source voltage.

Comparing the experimental results in Fig. 2 (e, f) with the simulations data in Fig. 3(a) reveals overall qualitative matching. The simulations managed to reproduce the shape of the IV-curve dip near zero gate-bias and the device threshold voltage V_{th} shift depending on the molecules' charge state due to the extra charge brought to the surface by the attachment of the molecules. In addition to the negative V_{th}-shift, the simulations also confirm the effect of the dip-widening with increasing the surface charge. However, the simulated absolute values are somewhat off, namely, they show: excessive negative V_{th}-shift and flipped asymmetry of the IV-curves compared to the experiment. Indeed, in the experiment the accumulated current is on average slightly larger than the inversion mode current, while in simulations, it is vice versa. The high sensitivity of the accumulation mode current to the tunneling non-local model parameters and lack of reliable experimental data for those parameters along with loosely defined floating potential of the device layer separated from the Source/Drain contacts by the Schottky/SiO2 barriers might be the reasons for the accumulated current underestimation in our simulations. More fine-tuning of the simulation model is needed to account for the on/off-current ratio mismatch, as the experimental ratio is 2–3 orders lower than the theoretical value. Hence, the surface recombination model needs to be improved. Part of the leakage current may be contributed by hoping conduction via the attached molecules spurious bypass channel, increasing the leakage current and reducing the effective on-/off-current ratio, which is not captured in simulations. All of this will be considered in our future work and further improvement of the computational model. Nevertheless, modeling only

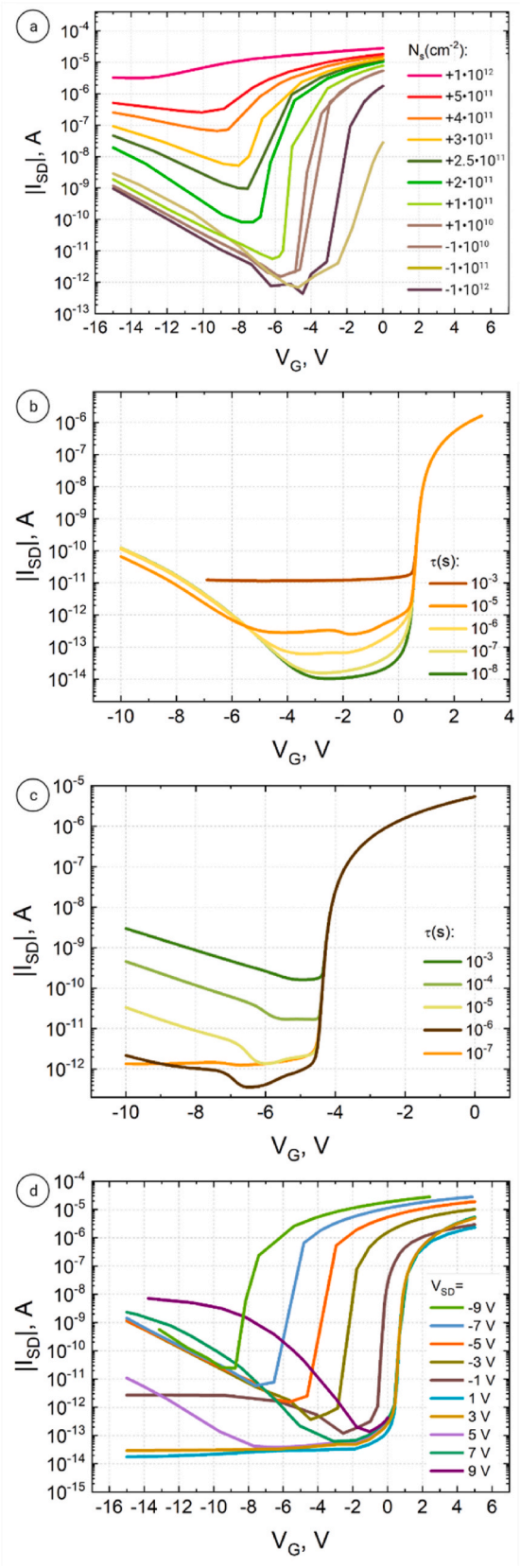

Fig. 3. Nanowire FET transfer characteristics for: (a) different effective surface charge; (b) different SRH recombination lifetimes of carriers in Si nano-wire of the FET device at the source-drain bias V_{SD} = - 5 V and (c) at V_{SD} = + 7 V; (d) different source-drain biases.

the effective surface charge at the silicon-air interface where the molecules are attached allows to describe the main features of the SiNW biosensor. Indeed, by relating the shift of the threshold voltage with respect to the relative change of the surface charge of the device from the simulation data one may calculate the conversion coefficient between the number of molecules attached to the sensor surface and the threshold voltage shift. This would provide a useful calibration tool for the bio-sensor and allow one to estimate the concentration of the molecules sensed by comparing the device IV-curves before and after the device exposure to their solution and benchmarking the V_{th} shift against the simulated curves family.

4. Conclusion

In this study, we developed back gate SiNW FET-based biosensor using the "top-down" nanofabrication approach. Fabricated SiNWs demonstrated good electrical characteristics after surface functionalization and further protein immobilization. After a protein attachment, the current was found to decrease, which is consistent with the appearance of a negative charge density on the surface of the silicon nanowire, which is also explained as a result of the complex effect of an effective negative shift of transistor IV-curve and associated device threshold voltage.

The simulations confirm the observed effect of the source-induced tunneling barrier lowering effect shifting the device threshold voltage. It also reduces the device's on-current at positive $V_{GS,}$ but this effect saturates at positive source voltages.

Comparing the experimental and simulated transfer IV-curves, we can conclude that the main mechanism of the effect of the detected Biotin-BSA complex on the corresponding properties of the transistor is an effective change in the source and gate bias caused by the nonzero electrical potential of the organic compound. The proposed version of the biosensor, distinguished by a relatively simple manufacturing method, a well-reproducible functionalization scheme, and an understandable electrical detection mechanism, seems to be a promising prototype for the implementation of detectors and sensors for important biological compounds.

Credit author statement

Tatyana E. Smolyarova: Conceptualization, Investigation, Data curation, Visualization, Writing – original draft preparation. **Lev V. Shanidze**: Investigation, Data curation, Formal analysis, Validation. **Anna V. Lukyanenko**: Methodology, Investigation, Resources. **Vasilisa V. Krasitskaya**: Methodology, Resources. **Anna S. Kichkailo**: Writing – review & editing. **Filipp A. Baron**: Software, Formal analysis, Validation, Writing – review & editing. **Anton S. Tarasov**: Project administration, Writing – review & editing and **Nikita V. Volkov**: Supervision.

Declaration of competing interest

The authors declare the following financial interests/personal relationships which may be considered as potential competing interests: Nikita Volkov reports financial support was provided by Russian Foundation for Basic Research. Anton Tarasov reports financial support was provided by Russian Foundation for Basic Research.

Acknowledgment

The reported study was funded by RFBR according to the research project N⁰ 20-32-90134. The authors thank RFBR, Krasnoyarsk Territory and Krasnoyarsk Regional Fund of Science (projects nos. 20-42-243007 and 20-42-240013) and the Government of the Russian Federation, Mega Grant for the Creation of Competitive World-Class Laboratories (Agreement no. 075-15-2019-1886) for financial support. Electron microscopy investigations were conducted with the help of

equipment of the Krasnoyarsk Territorial Shared Resource Center, Krasnoyarsk Scientific Center, Russian Academy of Sciences.

References

[1] C.Y. Hsiao, C.H. Lin, C.H. Hung, C.J. Su, Y.R. Lo, C.C. Lee, H.C. Lin, F.H. Ko, T. Y. Huang, Y.S. Yang, Novel poly-silicon nanowire field effect transistor for biosensing application, Biosens. Bioelectron. 24 (2009), https://doi.org/10.1016/j.bios.2008.07.032.

[2] P.C. Su, B.H. Chen, Y.C. Lee, Y.S. Yang, Silicon nanowire field-effect transistor as biosensing platforms for post-translational modification, Biosensors 10 (2020), https://doi.org/10.3390/BIOS10120213.

[3] D.P. Tran, T.T.T. Pham, B. Wolfrum, A. Offenhäusser, B. Thierry, CMOS-compatible silicon nanowire field-effect transistor biosensor: technology development toward commercialization, Materials 11 (2018), https://doi.org/10.3390/ma11050785.

[4] D. Li, H. Chen, K. Fan, V. Labunov, S. Lazarouk, X. Yue, C. Liu, X. Yang, L. Dong, G. Wang, A supersensitive silicon nanowire array biosensor for quantitating tumor marker ctDNA, Biosens. Bioelectron. 181 (2021), https://doi.org/10.1016/j.bios.2021.113147.

[5] S.I. Zida, C.C. Yang, Y.L. Khung, Y. Der Lin, Fabrication and characterization of an aptamer-based N-type silicon nanowire FET biosensor for VEGF detection, J. Med. Biol. Eng. 40 (2020), https://doi.org/10.1007/s40846-020-00552-5.

[6] S. Hemmilä, A. Gao, N. Lu, T. Li, Y. Wang, P. Kallio, Integration of microfluidic sample delivery system on silicon nanowire-based biosensor, Microsyst. Technol. 21 (2015), https://doi.org/10.1007/s00542-014-2076-0.

[7] J.S. Lee, S. Kim, K. Kim, T. Rim, Y.H. Jeong, M. Meyyappan, Nanoscale silicon ion-sensitive field-effect transistors for pH sensor and biosensor applications, in: 2011 IEEE Int. Conf. Electron Devices Solid-State Circuits, EDSSC, 2011, p. 2011, https://doi.org/10.1109/EDSSC.2011.6117562.

[8] G. Jayakumar, M. Östling, Pixel-based biosensor for enhanced control: silicon nanowires monolithically integrated with field-effect transistors in fully depleted silicon on insulator technology, Nanotechnology 30 (2019), https://doi.org/10.1088/1361-6528/ab0469.

[9] J.H. Lee, E.J. Chae, S. jeong Park, J.W. Choi, Label-free detection of γ-aminobutyric acid based on silicon nanowire biosensor, Nano Converg 6 (2019), https://doi.org/10.1186/s40580-019-0184-3.

[10] N. Lu, A. Gao, H. Zhou, Y. Wang, X. Yang, Y. Wang, T. Li, Progress in silicon nanowire-based field-effect transistor biosensors for label-free detection of DNA, Chin. J. Chem. 34 (2016), https://doi.org/10.1002/cjoc.201500857.

[11] X. Yang, Y. Fan, Z. Wu, C. Liu, A silicon nanowire array biosensor fabricated by complementary metal oxide semiconductor technique for highly sensitive and selective detection of serum carcinoembryonic antigen, Micromachines 10 (2019), https://doi.org/10.3390/mi10110764.

[12] T. Adam, A.M. Mohammed, T.S. Dhahi, N.F.B.N. Azua, N. Azizah, U. Hashim, S.C. B. Gopinath, Semiconductor nanowires biosensors for highly selective and multiplexed detection of biomolecules, J. Telecommun. Electron. Comput. Eng. 10 (2018).

[13] S. Kim, R. Lee, D. Kwon, T.H. Kim, T.J. Park, S.J. Choi, H.S. Mo, D.H. Kim, B. G. Park, Multiplexed silicon nanowire tunnel FET-based biosensors with optimized multi-sensing currents, IEEE Sensor. J. 21 (2021), https://doi.org/10.1109/JSEN.2021.3054052.

[14] A.V. Pawar, S.S. Kanapally, A.P. Chougule, P.P. Waifalkar, K.V. More, R.K. Kamat, T.D. Dongale, Simulation study of field-effect transistor based cylindrical silicon nanowire biosensor: effect of length and radius of the nanowire, J. Nano- Electron. Phys. 11 (2019), https://doi.org/10.21272/jnep.11(1).01005.

[15] A. Gao, S. Chen, Y. Wang, T. Li, Silicon nanowire field-effect-transistor-based biosensor for biomedical applications, Sensor. Mater. 30 (2018), https://doi.org/10.18494/SAM.2018.1829.

[16] S.M. Koo, M.D. Edelstein, Q. Li, C.A. Richter, E.M. Vogel, Silicon nanowires as enhancement-mode Schottky barrier field-effect transistors, Nanotechnology 16 (2005), https://doi.org/10.1088/0957-4484/16/9/011.

[17] T. Adam, U. Hashim, Highly sensitive silicon nanowire biosensor with novel liquid gate control for detection of specific single-stranded DNA molecules, Biosens. Bioelectron. 67 (2015), https://doi.org/10.1016/j.bios.2014.10.005.

[18] I. Lee, X. Luo, X.T. Cui, M. Yun, Highly sensitive single polyaniline nanowire biosensor for the detection of immunoglobulin G and myoglobin, Biosens. Bioelectron. 26 (2011), https://doi.org/10.1016/j.bios.2011.01.001.

[19] M.H. Jakob, B. Dong, S. Gutsch, C. Chatelle, A. Krishnaraja, W. Weber, M. Zacharias, Label-free SnO2 nanowire FET biosensor for protein detection, Nanotechnology 28 (2017), https://doi.org/10.1088/1361-6528/aa7015.

[20] M. Kaisti, Detection principles of biological and chemical FET sensors, Biosens. Bioelectron. 98 (2017), https://doi.org/10.1016/j.bios.2017.07.010.

[21] M. Getnet Yirak, R. Chaujar, TCAD analysis and modelling of gate-stack gate all around junctionless silicon NWFET based bio-sensor for biomedical application, in: Proc. 2nd Int. Conf. VLSI Device, Circuit Syst, VLSI DCS, 2020, p. 2020, https://doi.org/10.1109/VLSIDCS47293.2020.9179866.

[22] Y. Zhang, K. Han, J. Li, A simulation study of a gate-all-around nanowire transistor with a core-insulator, Micromachines 11 (2020), https://doi.org/10.3390/mi11020223.

[23] E. Mohammadi, N. Manavizadeh, An accurate TCAD-based model for ISFET simulation, IEEE Trans. Electron. Dev. 65 (2018), https://doi.org/10.1109/TED.2018.2857218.

[24] N. Ayadi, B. Hajji, H. Madani, A. Lale, J. Launay, P. Temple-Boyer, Modelling and performance evaluation of Si-NW ISFETmicrosensor, in: 2020 Int. Conf. Electr. Inf. Technol, ICEIT, 2020, p. 2020, https://doi.org/10.1109/ICEIT48248.2020.9113203.

[25] Y. Wang, G. Li, Simulation of a silicon nanowire FET biosensor for detecting biotin/streptavidin binding, in: 2010 10th IEEE Conf. Nanotechnology vol. 2010, NANO, 2010, https://doi.org/10.1109/NANO.2010.5697862.

[26] A. Bindal, S. Hamedi-Hagh, The design and analysis of dynamic NMOSFET/PMESFET logic using silicon nano-wire technology, Semicond. Sci. Technol. 21 (2006), https://doi.org/10.1088/0268-1242/21/8/003.

[27] A. Solanki, H. Um, Top-down etching of Si nanowires, in: Semicond. Semimetals, 2018, https://doi.org/10.1016/bs.semsem.2018.04.001.

[28] S. Barraud, B. Previtali, V. Lapras, R. Coquand, C. Vizioz, J.M. Hartmann, M. Cassé, Top-down fabrication and electrical characterization of Si and SiGe nanowires for advanced CMOS technologies, Semicond. Sci. Technol. 34 (2019), https://doi.org/10.1088/1361-6641/ab1e5b.

[29] L. Sekaric, O. Gunawan, A. Majumdar, X.H. Liu, D. Weinstein, J.W. Sleight, Size-dependent modulation of carrier mobility in top-down fabricated silicon nanowires, Appl. Phys. Lett. 95 (2009), https://doi.org/10.1063/1.3177331.

[30] R.S. Wagner, W.C. Ellis, Vapor-liquid-solid mechanism of single crystal growth, Appl. Phys. Lett. 4 (1964), https://doi.org/10.1063/1.1753975.

[31] F. Iacopi, P.M. Vereecken, M. Schaekers, M. Caymax, N. Moelans, B. Blanpain, O. Richard, C. Detavernier, H. Griffiths, Plasma-enhanced chemical vapour deposition growth of Si nanowires with low melting point metal catalysts: an effective alternative to Au-mediated growth, Nanotechnology 18 (2007), https://doi.org/10.1088/0957-4484/18/50/505307.

[32] I. Zardo, S. Conesa-Boj, S. Estradé, L. Yu, F. Peiro, P. Roca I Cabarrocas, J. R. Morante, J. Arbiol, A. Fontcuberta I Morral, Growth study of indium-catalyzed silicon nanowires by plasma enhanced chemical vapor deposition, Appl. Phys. Mater. Sci. Process 100 (2010), https://doi.org/10.1007/s00339-010-5802-1.

[33] E.E. Bashmakova, A.N. Kudryavtsev, L.A. Frank, Development of the method to produce functionally active recombinant streptavidin in escherichia coli cells, J. Sib. Fed. Univ. - Biol. 13 (2020), https://doi.org/10.17516/1997-1389-0324.

[34] T.E. Smolyarova, A.V. Lukyanenko, A.S. Tarasov, L.V. Shanidze, F.A. Baron, F. V. Zelenov, I.A. Yakovlev, N.V. Volkov, Biosensors based on nanowire field effect transistors with Schottky contacts, J. Phys. Conf. Ser. (2019), https://doi.org/10.1088/1742-6596/1410/1/012013.

[35] A.S. Tarasov, A.V. Lukyanenko, I.A. Bondarev, M.V. Rautskii, F.A. Baron, T. E. Smolyarova, I.A. Yakovlev, S.N. Varnakov, S.G. Ovchinnikov, N.V. Volkov, Fabrication and DC/AC characterization of 3-terminal ferromagnet/silicon spintronics devices, Semiconductors 52 (2018), https://doi.org/10.1134/S1063782618140312.

[36] C.M. Dundas, D. Demonte, S. Park, Streptavidin-biotin technology: improvements and innovations in chemical and biological applications, Appl. Microbiol. Biotechnol. 97 (2013), https://doi.org/10.1007/s00253-013-5232-z.

[37] S. Cristoloveanu, From SOI Basics to Nano-Size MOSFETs. https://doi.org/10.1007/978-0-387-49965-9_2, 2007.

[38] O.V. Naumova, B.I. Fomin, D.A. Nasimov, N.V. Dudchenko, S.F. Devyatova, E. D. Zhanaev, V.P. Popov, A.V. Latyshev, A.L. Aseev, Y.D. Ivanov, A.I. Archakov, SOI nanowires as sensors for charge detection, Semicond. Sci. Technol. 25 (2010), https://doi.org/10.1088/0268-1242/25/5/055004.

[39] N.A. Taranova, V.D. Slobodenuyk, A.V. Zherdev, B.B. Dzantiev, Network of gold conjugates for enhanced sensitive immunochromatographic assays of troponins, RSC Adv. 11 (2021), https://doi.org/10.1039/d1ra02212a.

[40] R.E. Bank, D.J. Rose, Global approximate Newton methods, Numer. Math. 37 (1981), https://doi.org/10.1007/BF01398257.

[41] C.C. Mcandrew, K. Singhal, E.L. Heasell, A consistent nonisothermal extension of the scharfetter-gummel stable difference approximation, IEEE Electron. Device Lett. 6 (1985), https://doi.org/10.1109/EDL.1985.26187.

[42] A. Schenk, G. Heiser, Modeling and simulation of tunneling through ultra-thin gate dielectrics, J. Appl. Phys. 81 (1997), https://doi.org/10.1063/1.365364.

[43] L.F. Register, E. Rosenbaum, K. Yang, Analytic model for direct tunneling current in polycrystalline silicon-gate metal-oxide-semiconductor devices, Appl. Phys. Lett. 74 (1999), https://doi.org/10.1063/1.123060.

[44] G.A.M. Hurkx, D.B.M. Klaassen, M.P.G. Knuvers, A new recombination model for device simulation including tunneling, IEEE Trans. Electron. Dev. 39 (1992), https://doi.org/10.1109/16.121690.